The South Pacific Meridional Mode: A Mechanism for ENSO-like Variability

HONGHAI ZHANG AND AMY CLEMENT

Rosenstiel School of Marine and Atmospheric Science, University of Miami, Miami, Florida

PEDRO DI NEZIO

International Pacific Research Center, University of Hawai'i at Mānoa, Honolulu, Hawaii

(Manuscript received 5 February 2013, in final form 9 July 2013)

ABSTRACT

In this study, the authors investigate the connection between the South Pacific atmospheric variability and the tropical Pacific climate in models of different degrees of coupling between the atmosphere and ocean. A robust mode of variability, defined as the South Pacific meridional mode (SPMM), is identified in a multimodel ensemble of climate model experiments where the atmosphere is only thermodynamically coupled to a slab ocean mixed layer. The physical interpretation of the SPMM is nearly identical to the North Pacific meridional mode (NPMM) with the off-equatorial southeast trade wind variability altering the latent heat flux and sea surface temperature (SST) and initiating a wind–evaporation–SST feedback that propagates signals into the tropics. The authors also show that a positive cloud feedback plays a role in the development of this mode, but this effect is model dependent. While physically analogous to the NPMM, the SPMM has a stronger expression in the equatorial Pacific and directly perturbs the zonal gradients of SST and sea level pressure (SLP) on the equator, thus leading to ENSO-like variability despite the lack of ocean–atmosphere dynamical coupling. Further analysis suggests that the SPMM is also active in fully coupled climate models and observations. This study highlights the important role of the Southern Hemisphere in tropical climate variability and suggests that including observations from the data-poor South Pacific could improve the ENSO predictability.

1. Introduction

The influence of mid-to-high latitude atmospheric variability on the tropical Pacific climate has been investigated over the past decade with a primary goal of improving the prediction of El Niño–Southern Oscillation (ENSO). The focus of this topic has been the connection of the North Pacific to the tropics. The North Pacific Oscillation (NPO), a mode of atmospheric variability over the North Pacific (Rogers 1981), has been identified as a possible driver of the tropical Pacific climate variability on the seasonal time scale (Vimont et al. 2001, 2003a,b, 2009; Chiang and Vimont 2004; Chang et al. 2007). The physical processes connecting the NPO and tropical Pacific variability were first explained by Vimont et al. (2001, 2003a,b) as the "seasonal footprinting mechanism." By modulating the northeast trade winds on its southern flank during boreal winter, the NPO can leave an anomalous footprint in sea surface temperature over the northeast subtropical Pacific through latent heat flux changes, which persist into boreal summer and in turn induce atmospheric circulation changes in the tropical Pacific. Motivated by the similarities between the Pacific and Atlantic climatology and the well-established Atlantic meridional mode (Chang et al. 1997), Chiang and Vimont (2004) demonstrated the existence of the equivalent North Pacific meridional mode (NPMM) and provided it with a physical interpretation that is identical to the seasonal footprinting mechanism but has no intrinsic time scales. By presenting observational evidence that most El Niño events in the past four decades are preceded by strong NPMM activity (positive phase), Chang et al. (2007) argued that the NPMM operates as an effective conduit through which the North Pacific variability, particularly the NPO, triggers ENSO. In addition, those authors as well as Vimont et al. (2009) performed numerical experiments to show that the seasonality

Corresponding author address: Honghai Zhang, Rosenstiel School of Marine and Atmospheric Science, University of Miami, 4600 Rickenbacker Cswy., Miami, FL 33149.
E-mail: hzhang@rsmas.miami.edu

DOI: 10.1175/JCLI-D-13-00082.1

© 2014 American Meteorological Society

of midlatitude atmospheric variability and subtropical air–sea thermodynamic coupling in the North Pacific plays a fundamental role in the seasonal phase-locking behavior of ENSO, suggesting impacts on ENSO seasonality from the Northern Hemisphere. On longer than interannual time scales, extratropical Pacific decadal variability has also been shown to modulate the tropical Pacific low frequency variability via both atmospheric (Barnett et al. 1999) and oceanic (Pierce et al. 2000) teleconnections.

There are, on the other hand, few studies that investigate the influences of the southern mid-to-high latitude variability on the tropical Pacific. An early study by van Loon and Shea (1985) suggested that the Southern Oscillation (SO) may originate in the South Pacific. They showed that the trough in the midlatitude westerlies of the South Pacific weakens in latitudes equatorward of 45°S during austral fall and winter of the year before the SO warm events, resulting in weaker meridional winds across the entire Pacific in latitudes between 45° and 15°S, which warm the surface below. Those authors argued the interaction between the seasonal development of the South Pacific convergence zone (SPCZ) and the anomalously warm ocean below enhances low pressure in the subtropics and leads to development of the SO. Later, van Loon et al. (2003) presented a case study of the SO warm events in the early 1990s, which exhibits a development of SLP anomalies over the south subtropical Pacific similar to that described in van Loon and Shea (1985).

Southern extratropical variability outside the South Pacific has also been proposed to impact the tropical Pacific. Terray and Dominiak (2005) found a change in the lead–lag relationship between the southeast Indian Ocean SST and ENSO evolution associated with the 1976–77 climate regime shift and suggested that the southeast Indian Ocean SST variability can be a key precursor of ENSO events by remotely affecting the South Pacific midlatitude atmospheric circulation via Rossby wave dynamics. How the South Pacific midlatitude fluctuations then influence the tropical Pacific was not answered in that study. A more recent study by Terray (2010) showed that observed subtropical variability in both the south Indian and South Atlantic Oceans originating from the Southern Hemisphere midlatitudes may exert a substantial impact on ENSO. The subtropical cold SST anomalies in the south Indian and South Atlantic Oceans extend into the deep tropics of those basins via a feedback between the SST gradient, surface winds, and latent heat fluxes—akin to the NPMM. Then all three tropical basins are connected through atmospheric teleconnections: the weakened convection in the equatorial Atlantic and Indian Ocean forces a cold equatorial Kelvin wave in the mid to upper troposphere that propagates eastward into the western equatorial Pacific, where it results in persistent anomalous convection and surface westerlies by reducing atmospheric stability. Terray further argued that these anomalies over the western equatorial Pacific may trigger an El Niño event. An observed subtropical variability pattern in the South Pacific, similar to those in the south Indian and South Atlantic Oceans, has also been documented by Wang (2010a), but whether it can influence the tropical Pacific is unknown.

These observational results have support from idealized modeling experiments. Matei et al. (2008) investigated the subtropical forcing of the tropical Pacific climate by imposing anomalous surface warming/cooling over the subtropical South and North Pacific separately in a single climate model [Max Planck Institute (MPI) ECHAM5]. They found that the subtropical South Pacific anomalies have a stronger and faster impact on the tropical Pacific mainly through atmosphere–mixed layer interactions, in contrast to the slower ocean dynamic processes for the subtropical North Pacific. Using a different climate model [Hadley Centre Coupled Model, version 3 (HadCM3)], Toniazzo (2009) found that about 40% of the simulated ENSO variability is related to the southeast tropical Pacific variability between 5° and 17°S, which tends to precede the equatorial ENSO anomaly by a few months, implying a possible South Pacific origin of ENSO in that model.

These prior studies have used observations or a single climate model to identify the linkage between the South Pacific mid-to-high latitude variability and the tropical Pacific variability. In this study we will investigate the physical mechanisms of this linkage in multiple AGCMs coupled with a slab ocean (hereafter AGCM-slab models). Fully coupled climate model simulations and observations will be used to test our findings.

2. Data and methodology

We focus on the simulation of climate variability in the AGCM-slab models. The advantage of using these models is that it removes the tropical Pacific variability associated with dynamical coupled ocean–atmosphere interactions, which are fairly well understood, and allows us to examine other mechanisms of variability. There are a number of studies that have attempted to remove ENSO in various ways [see Compo and Sardeshmukh (2010) and the references therein], but complete removal of ENSO influence is challenging owing to the nonlinear interaction between ENSO and non-ENSO phenomena. The AGCM-slab ocean framework provides, perhaps, the cleanest way to remove ENSO by excluding

TABLE 1. Statistics of the models used in this study. The standard deviation of the TCW is defined as that of the Southern Oscillation index (monthly sea level pressure difference between 5°S–5°N, 100°E–180° and 5°S–5°N, 90°–140°W) in the AGCM-slab models (Clement et al. 2011).

Acronym	Model	Simulation length Slab/PIcntrl (yr)	Std dev of TCW (Pa)
CCCma	Canadian Centre for Climate Modelling and Analysis	30/1001	42
CCCma T63	Canadian Centre for Climate Modelling and Analysis T63	30/350	43
GFDL CM2.0	Geophysical Fluid Dynamics Laboratory Climate Model, version 2.0	50/500	51
GFDL CM2.1	Geophysical Fluid Dynamics Laboratory Climate Model, version 2.1	100/500	61
INM-CM3.0	Institute of Numerical Mathematics Coupled Model, version 3.0	60/330	31
MIROC (hires)	Model for Interdisciplinary Research on Climate, version 3.2 (high resolution)	20/100	45
MIROC (medres)	Model for Interdisciplinary Research on Climate, version 3.2 (medium resolution)	60/500	46
MPI ECHAM5	Max Planck Institute ECHAM5	100/506	72
MRI CGCM2.3.2a	Meteorological Research Institute Coupled General Circulation Model, version 2.3.2a	150/150	55
NCAR CCSM4	National Center for Atmospheric Research Community Climate System Model, version 4	540/500	43
HadGEM1	Hadley Centre Global Environmental Model, version 1	70/172	76

the dynamical coupling between the ocean and atmosphere that gives rise to ENSO. In this framework, SST is simulated by the thermodynamic equation

$$\rho h C_p \frac{\partial T}{\partial t} = Q_{\text{net}} + Q_{\text{flux}},$$

where ρ, C_p, and T are seawater density, specific heat at constant pressure, and temperature (i.e., SST), respectively; h is the slab ocean depth; and Q_{flux} is a prescribed seasonally varying term, representing the climatological ocean heat flux convergence underneath the surface mixed layer. This term contributes to the seasonal cycle of SST but does not drive the interannual variability. In the equation, Q_{net} is the net sea surface heat flux, consisting of latent and sensible heat fluxes as well as shortwave and longwave radiation. The shortwave plus longwave radiation can be separated into cloud and clear-sky radiation to highlight the role of clouds.

Here we analyze control simulations of 11 AGCM-slab models (see Table 1 for a list of the models), 10 of which are archived in the World Climate Research Programme (WCRP) Coupled Model Intercomparison Project phase 3 (CMIP3) and made available through the Program for Climate Model Diagnostics and Intercomparison (PCMDI). These 10 AGCM-slab models have a constant 50-m slab ocean depth and include the CCCma, CCCma T63, GFDL CM2.0, GFDL CM2.1, INM-CM3.0, MIROC (hires), MIROC (medres), MPI ECHAM5, MRI CGCM2.3.2a, and HadGEM1. The other AGCM-slab model used in this work is the Community Atmosphere Model (CAM, version 4) coupled with a slab ocean that is developed at National Center for Atmospheric Research (NCAR CCSM4). The slab ocean depth in NCAR CCSM4 is spatially dependent but temporally constant and is derived from the annual-mean conditions of a preindustrial control (PIcntrl) simulation of the fully coupled model (i.e., CCSM4). We find that the results from NCAR CCSM4 are similar to those in other models, suggesting that the spatially varying slab ocean depth does not affect the main conclusions of this paper.

In addition, we also use preindustrial control simulations of the fully coupled climate models corresponding to the 10 AGCM-slab models archived in CMIP3, as well as CCSM4 archived in CMIP5. We further include observations of monthly SST and SLP from the Met Office (UKMO) (Rayner et al. 2003), extended reconstructed SST, version 3 (ERSST v3), from the National Oceanic and Atmospheric Administration (NOAA) Earth System Research Laboratory (Smith et al. 2008), surface wind reanalysis from National Centers for Environmental Prediction (Kalnay et al. 1996), and precipitation product from Global Precipitation Climatology Project, version 2.2 (Adler et al. 2003). Due to the lack of observations in the South Pacific before the satellite era, the data only after 1979 is used in this study.

3. Results

The linkages between the North/South Pacific and the equatorial climate can be visualized by the regression of

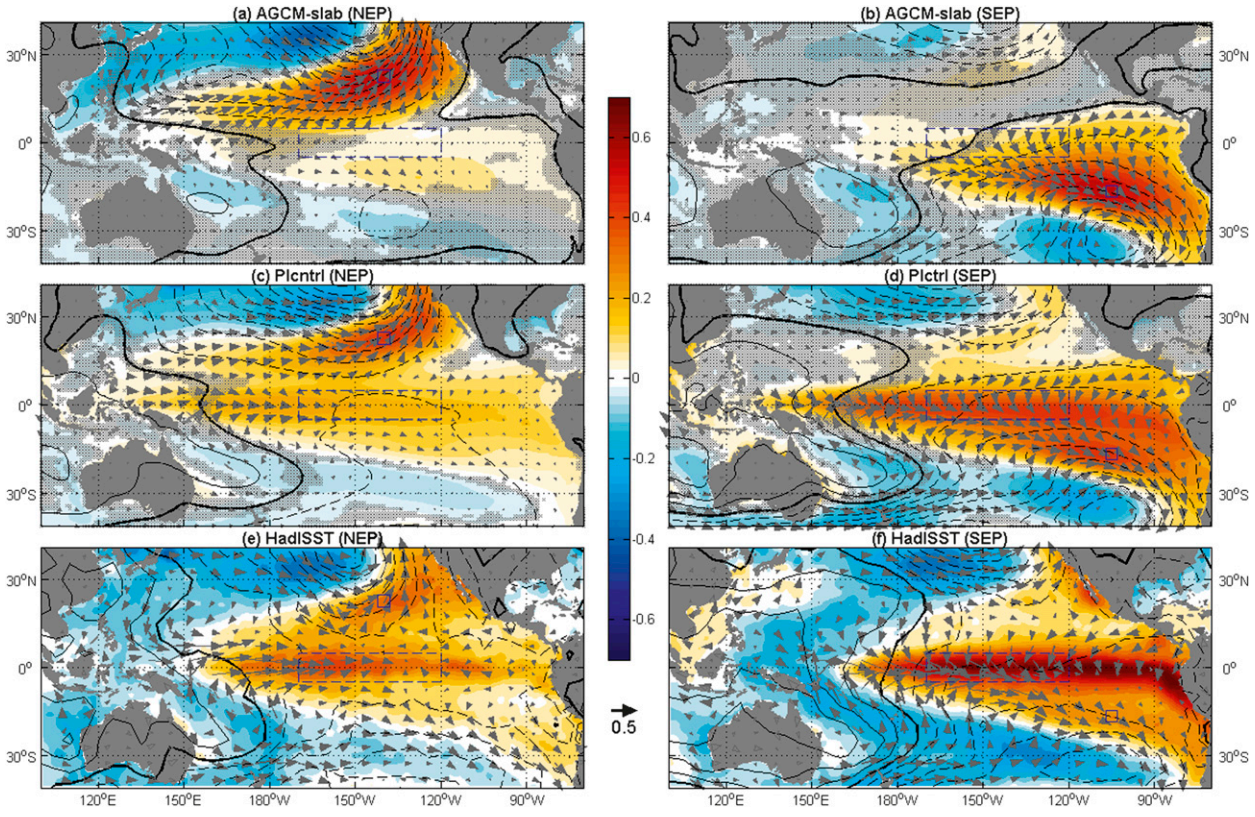

FIG. 1. Regression of anomalous SST (shading), SLP (contours), and surface winds (arrows) onto normalized SST time series averaged in the (left) northeast (21°–25°N, 138°–142°W) and (right) southeast (19°–15°S, 103°–107°W) Pacific, respectively. (a),(b) The multimodel mean of 11 AGCM-slab models; (c),(d) as in (a) but for the fully coupled version (preindustrial scenario); and (e),(f) observation. All panels share the same color scale and all arrows are plotted relative to the same scale vector (0.5 m s^{-1}). Negative (positive) SLP contours are dashed (solid) with zero SLP contours in thick solid lines: contour interval 10 Pa. Anomaly is derived by removing seasonal cycle and linear trend (for observation only) and applying a 1.5-yr low-pass filter. Gray hatched area in the top two rows means the multimodel mean is not significant, where the significance is defined when at least 8 out of 11 models have the same sign as the multimodel mean. Observations include SST and SLP data from the Met Office and surface wind reanalysis data from National Centers for Environmental Prediction. Results based on NOAA ERSST are similar.

SST, sea level pressure (SLP), and surface winds onto normalized SST anomaly time series averaged over the northeast (21°–25°N, 138°–142°W) and southeast (19°–15°S, 103°–107°W) Pacific, respectively. Figures 1a and 1b show the multimodel mean regression of the 11 AGCM-slab models. The pattern that emerges for the Northern Hemisphere (Fig. 1a) is identical to the NPMM. It clearly exhibits the anomalous SST footprint in the northeast subtropical Pacific caused by surface trade wind variability associated with the NPO and the SST-induced zonal wind anomalies in the west tropical Pacific through the wind–evaporation–SST (WES) feedback (Xie and Philander 1994). These zonal wind anomalies, in the presence of ocean dynamics, can be amplified by the positive Bjerknes feedback and, thus, trigger ENSO events (Chang et al. 2007; Vimont et al. 2009). The regression pattern for the Southern Hemisphere (Fig. 1b) has remarkably similar characteristics including a maximum SST signal oriented with the southeast trade wind variations, which suggests a possible source of midlatitude forcing of the tropical Pacific from the Southern Hemisphere. By analogy, we define this pattern (Fig. 1b) as the South Pacific meridional mode (SPMM) and will demonstrate in this section that the SPMM has a similar physical interpretation with the NPMM. We explore the sensitivity of the regression patterns to the location and size of the box used to compute the SST index, and the results are similar. We also compute the joint empirical orthogonal function decomposition of the covariance between SST and SLP in the South Pacific and obtain a pattern similar to Fig. 1b as well (not shown).

In addition to the similarities, there also exist some noticeable differences between the northern and southern regression patterns. The most interesting is that, in the AGCM-slab models, the variability in the Southern

Hemisphere extends onto the east-to-central equatorial Pacific and affects the zonal gradient of SST and SLP on the equator, while the northern variability appears to be more confined to the Northern Hemisphere and only affects the northwest subtropical Pacific. Further, because of the zonal asymmetries on the equator in SST and SLP, the SPMM has an ENSO-like spatial structure (Zhang et al. 1997) that bears strong resemblance to the thermally coupled Walker mode (TCW) proposed in a recent study by Clement et al. (2011). The TCW refers to the ENSO-like variability on interannual to decadal time scales in the absence of ocean–atmosphere dynamical coupling and is shown to be a robust feature emerging in different AGCMs coupled with a slab ocean from the CMIP3 archive. Those authors hypothesized a fundamental role of trade wind variability in the TCW. Yet the detailed physical mechanisms underlying the TCW were not addressed in that study. We will also show in this study that the SPMM to a large extent accounts for the TCW.

a. Composites of SPMM warm events

A composite heat budget analysis is applied to examine the evolution of warm events in the southeast subtropical Pacific in individual AGCM-slab models and their multimodel mean. In each model, we use the SST index averaged in the southeast Pacific (25°–15°S, 110°–90°W: referred to as SEP index) to determine the peaks of the warm events, and we analyze the 3 years prior to and subsequent to those peaks. Warm ''events'' are chosen when the SST indices exceed one standard deviation and are used in the composite analysis. The climatological seasonal cycle is removed from all fields and a low-pass filter with a cutoff period of 1.5 yr is applied to remove the high frequency variability and focus on the interannual time scales. Similar analyses are performed on high-pass filtered as well as unfiltered data, and the results are similar except for the temporal characteristics (see more discussion below). Before computing the composite heat budget in each model, we normalize all fields by the standard deviation of the SEP index. In this way, the composite warm event in each model is relative to one standard deviation of the variability of the SEP index and is used to calculate the multimodel mean. The results presented here are not sensitive to the normalization. Note that the SEP index is computed for an area larger than that of the SST index used in the regression. This is because the SST regression signal emerges in a broader spatial scale (Fig. 1b) and a composite index averaged for a larger area can better capture the large-scale processes responsible for the SPMM. However, as mentioned before, the results presented here are not sensitive to the SST index used.

In the initial stage of development (Fig. 2a, $t = -12$; i.e., 12 months before the SEP index peak), the southeast (SE) Pacific warms along with an anomalous cyclone present in the SE Pacific. Over the course of the event, the warming and SLP signals strengthen and expand northward and westward. At the peak of the SPMM warm event (Fig. 2a, $t = 0$), the SST anomalies exhibit an ENSO-like pattern of surface warming in the eastern Pacific with its maximum occurring to the south of the equator (around 15°S, 110°W). Correspondingly, the anomalous SLP pattern shows a zonal dipole structure on the equator that strongly resembles the TCW [cf. Fig. 6c in Clement et al. (2011)] and also the real world Southern Oscillation. After the mature phase, the maximum surface warming as well as the anomalous cyclone move northward onto the equator and expand northwestward (Fig. 2a, $t = +6$), and the warming in the Niño-3.4 region peaks.

The ENSO-like structure appearing in the composites, particularly after the developed phase of the SPMM, suggests that the physical processes generating the SPMM should also, at least in part, be responsible for the thermally coupled Walker mode (i.e., the ENSO-like variability in the absence of ocean–atmosphere dynamical coupling).

b. Mechanisms

To illustrate the mechanisms underlying the composite SPMM warm event described above, we present the maps of composite cloud radiation and latent heat flux anomalies in Fig. 2 (center and right). The clear-sky radiation and sensible heat flux anomalies are generally much smaller in magnitude, and thus not shown here. All heat fluxes are defined such that positive corresponds to warming the surface.

The initial surface warming around $t = -12$ near 20°S in the SE Pacific is primarily due to the weakening of off-equatorial trade winds and positive latent heat flux anomalies (Fig. 2c, $t = -12$). With warmer temperatures and a weaker subtropical high in the SE subtropical Pacific, the southeast trade winds further weaken, including weaker cross-equatorial flow in the eastern equatorial Pacific, which in turn strengthens the surface warming via enhanced latent heat flux anomalies (Fig. 2c, $t = -6$). There is also warming from positive cloud radiation anomalies owing to reduced cloud over in the eastern equatorial–southeast subtropical Pacific and cooling associated with increased cloud cover to the south in the center of the anomalous cyclone (Fig. 2b, $t = -6$), which tends to shift the SST anomaly northward. At the peak of the event ($t = 0$), the latent heat flux becomes negative (cooling) in the region of maximum surface warming (around 20°S, 95°W) in spite of

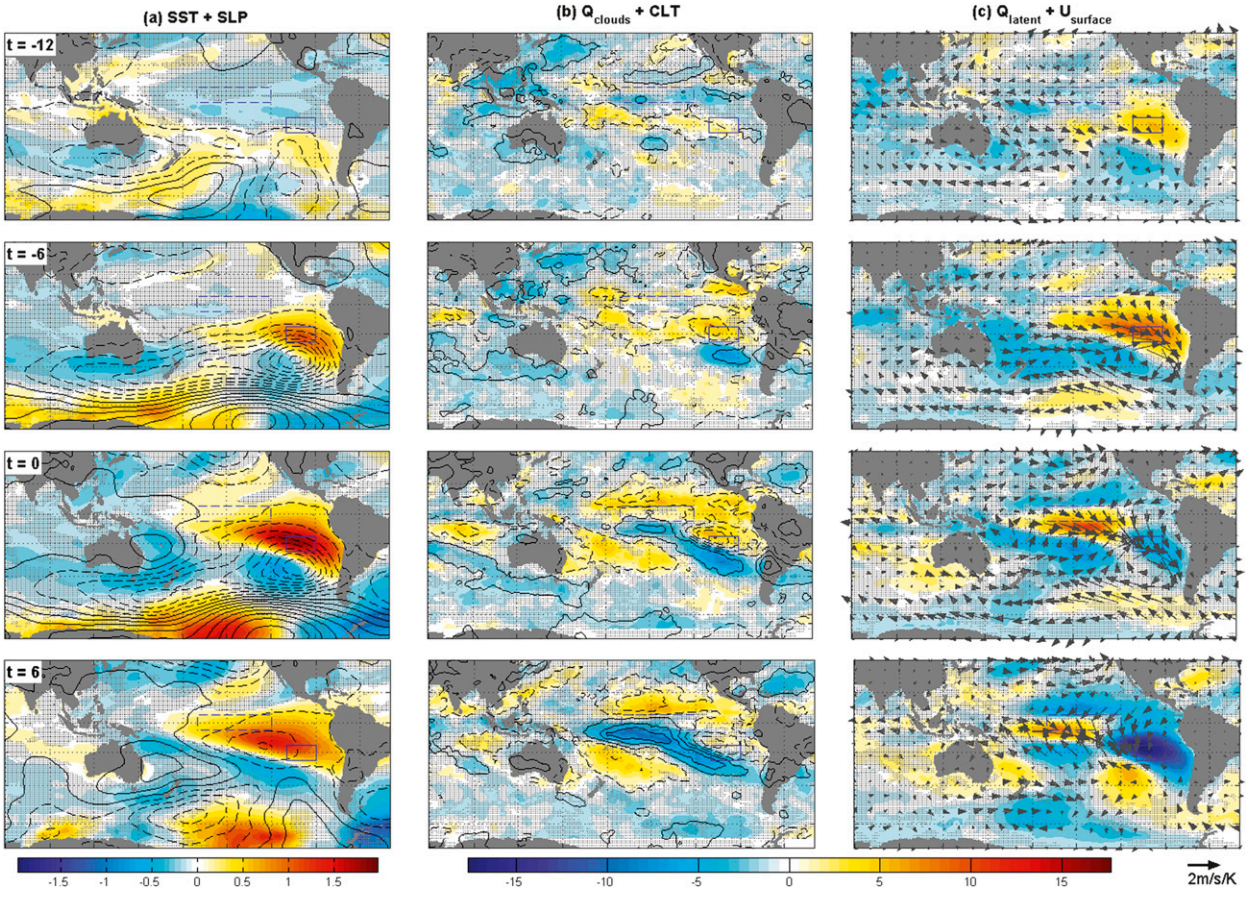

FIG. 2. Multimodel (AGCM-slab) mean composite maps of anomalous (left) SST and SLP, (center) cloud radiation and total cloud cover (CLT), and (right) latent heat flux and surface wind at times −12, −6, 0, and +6 months relative to the peak of SE Pacific SST index (averaged over 25°–15°S, 110°–90°W; see the solid blue box). SST and individual heat flux components are plotted in shading while SLP, CLT in contours, respectively. Solid (dashed) contours denote positive (negative) anomaly; zero contours are omitted. The contour intervals of SLP and CLT are 40 Pa K^{-1} and 2% K^{-1} (normalized by the SEP index standard deviation), respectively. Latent heat flux and cloud radiation share the same color scale (bottom right). Gray hatched area means the multimodel mean is not significant, where the significance is defined when at least 8 out of 11 models have the same sign as the multimodel mean. The heat flux anomaly is positive downward.

the weakened surface trade winds (Fig. 2c, $t = 0$). This is because of the strong dependence of latent heat flux on SST via specific humidity[1] (Wang 2010b). However, in the eastern equatorial–southeast subtropical region (north of 20°S), there is a positive cloud feedback (Fig. 2b, $t = 0$), which to some extent offsets the latent heat flux damping. We point out that clouds involved in the positive cloud feedback simulated in CMIP3 models are not necessarily the prevailing low-level stratus in the eastern Pacific basin owing to the cloud parameterizations in these models (Clement et al. 2010).

Negative latent heat flux anomalies lead to the decay of the warm event in the eastern basin (Fig. 2c, $t = 6$). As the negative latent heat flux anomalies develop in the SE Pacific, positive latent heat flux anomalies along with the weakened trade winds propagate northwestward into the western-central equatorial Pacific around the date line (Fig. 2c, $t = 0$). This process suggests the WES feedback, which accounts for the delayed peak of the surface warming in the Niño-3.4 region compared to the SE Pacific. The northwestward propagation associated with the WES feedback can also be seen from the composite SST and SLP Hovmöller diagram (see Fig. 3a)

[1] The latent heat flux in models is calculated via the bulk formula $Q_{LH} = C_0 U(q_s(T) - q(T))$, where C_0 is constant, U is the surface wind speed, and the specific humidity $q(T)$ is a function of SST (T). The latent heat flux anomaly ΔQ_{LH} thus can be simply expressed as $\Delta Q_{LH} = (\partial Q_{LH}/\partial U)\Delta U + (\partial Q_{LH}/\partial T)\Delta T$. It can be seen that both surface wind anomaly (ΔU) and SST anomaly (ΔT) can lead to the latent heat flux anomaly. During the initial stage of the composite SPMM warm event, the surface warming is weak and ΔQ_{LH} is caused by ΔU. Around the peak of the event, the surface warming is strong and dominates ΔQ_{LH}.

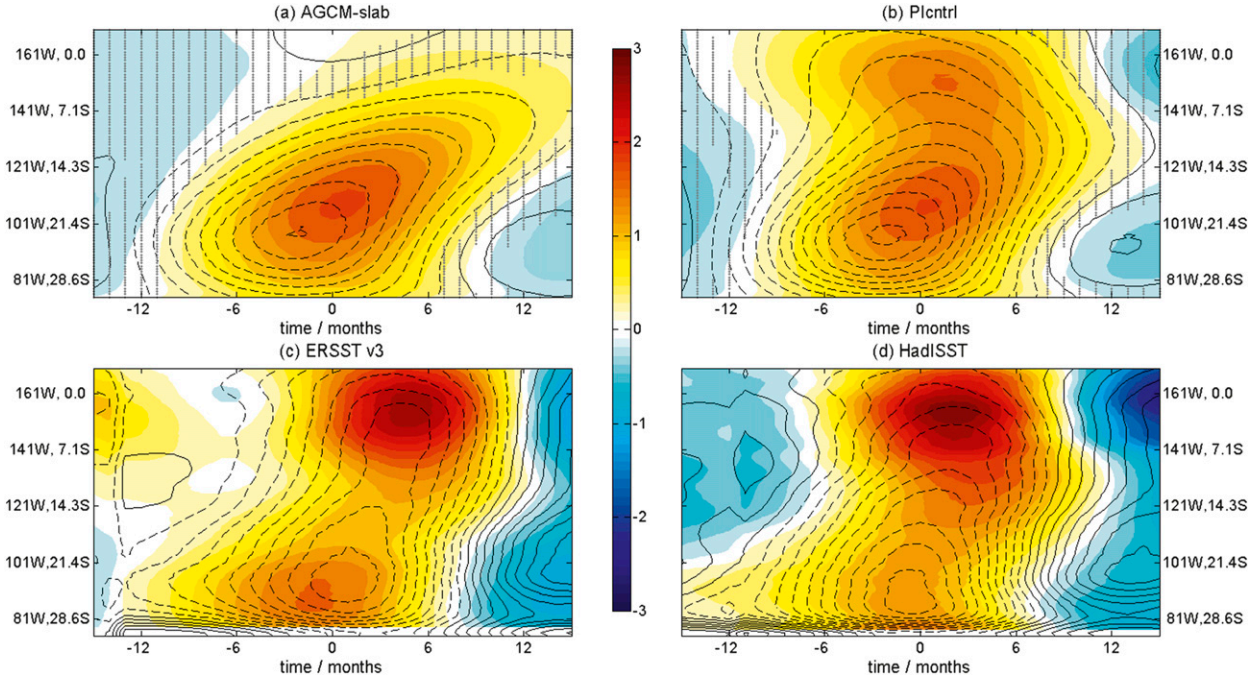

FIG. 3. Composite Hovmöller diagram along a tilted straight line (y axis) connecting SE Pacific (28.6°S, 81°W) to central equatorial Pacific (0°, 161°W) in (a) AGCM-slab models, (b) fully coupled climate models and observations, (c) NOAA ERSST v3, and (d) Hadley Centre SST. Color is composite SST anomaly and contours SLP. The SLP in (c) and (d) is from the Hadley Centre but based on the composite SEP index derived from ERSST and HadISST, respectively. The x axis indicates the lead/lag time (month) relative to the peak of the SEP index. Hatched area in the top row denotes that the multimodel mean is not significant (see Fig. 2 caption for the definition of significance).

plotted along a tilted straight line connecting the SE Pacific (28.6°S, 81°W) to the central equatorial Pacific (0°, 161°W). The Hovmöller diagram clearly shows the northwestward development of the surface warming as well as the anomalous cyclone. The WES feedback plays a fundamental role in propagating the southern extratropical variability onto the equator in the AGCM-slab models, which is identical to the propagation mechanism of the NPMM (Vimont et al. 2009). In the western-central Pacific, the latent heat flux warming is largely offset by the radiative cooling from clouds (Fig. 2b, $t = 0$), and the surface warming is small. In contrast to the positive cloud feedback in the eastern Pacific, clouds in the western-central Pacific act mainly as a damping mechanism. This western-central Pacific cloud damping amplifies the zonal asymmetry of the warm event.

To further illustrate the mechanisms of the composite warm event, we analyze the domain-averaged composite heat budget in the east equatorial–southern subtropical Pacific (EESSP; 20°S~10°N, 120°~80°W). The multimodel mean is shown in Fig. 4a and verifies the physical mechanisms of the SPMM described above. The surface warming (thick red curve) in the EESSP is initiated by the positive latent heat flux anomaly (green curve), caused by the weakened surface trade winds (gray curve), and then grows with the positive cloud radiation anomaly (blue curve) via the positive cloud feedback. As the surface warming intensifies, the latent heat flux anomaly becomes negative owing to the warmer surface temperature (despite weaker surface winds) and is responsible for the decay of the warm event.

The composite events show a time scale of approximately 1–2 yr; however, this should not be interpreted as a preferred time scale of this mode. Rather, it represents the average duration of events because the spectrum of variability in the AGCM-slab models is red (Clement et al. 2011). The results presented here focus on the interannual time scales due to the application of the low-pass filter (with the cutoff period of 1.5 yr). We also perform the same composite analysis on high-pass filtered as well as unfiltered data and find similar physical processes on *shorter-than-interannual* time scales as well (not shown).

While the off-equatorial trade wind variability in the SE Pacific and its effect on latent heat flux are simulated in all individual models, the positive cloud feedback in the EESSP area is not, which suggests that the positive cloud feedback is not fundamental to the SPMM. To illustrate the differences between models, we also show the domain-averaged composite heat budget analysis in

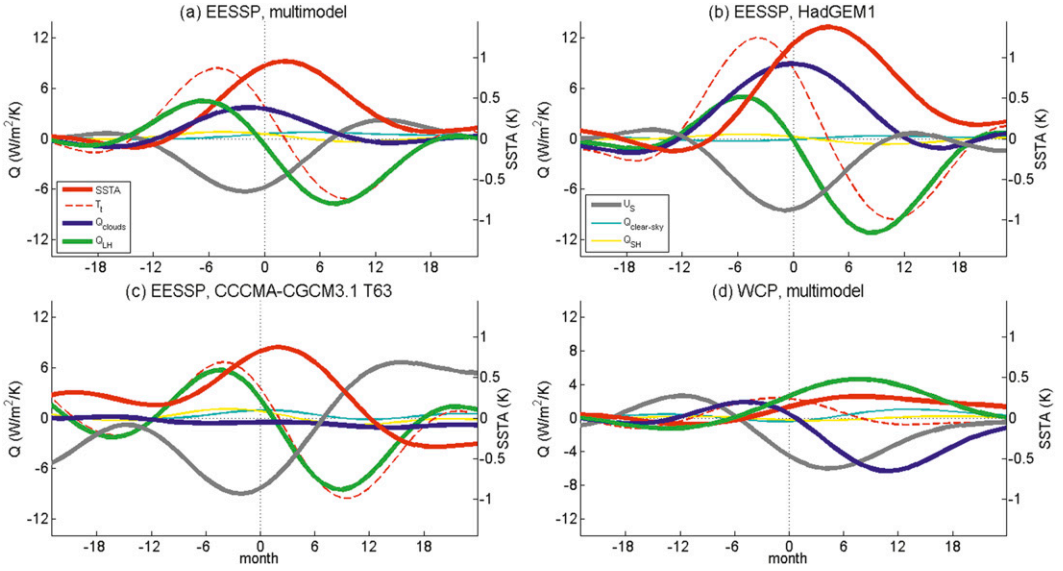

FIG. 4. Composite heat budget analysis averaged over the (a)–(c) EESSP (10°N ~ 20°S, 80° ~ 120°W) and the (d) western-central Pacific (10°S ~ 0°, 160°E ~ 160°W) in AGCM-slab models. The *x* axis denotes the lead/lag time (month) relative to the peak of SE Pacific SST index. The SST anomaly is plotted in thick red line with its tendency in dashed red line and cloud radiation, latent heat flux, clear-sky radiation, and sensible heat flux anomaly in thick blue, green, thin cyan, and yellow lines, respectively. The surface wind speed anomaly (gray line) is multiplied by $5\,\mathrm{W\,s\,m^{-3}\,K^{-1}}$ in order to share the same *y* axis on the left as heat fluxes. Panels (a)–(c) indicate the composite heat budget for the multimodel mean, UKMO HadGEM1, and CCCma T63 in the EESSP, respectively; (d) is for the multimodel mean in the western-central Pacific. UKMO HadGEM1 simulates a significant positive feedback between the SST and low-level clouds in the EESSP, while CCCma T63 does not.

HadGEM1 that simulates the positive cloud feedback (Fig. 4b) and in CCCma T63 that does not (Fig. 4c) [see Clement et al. (2009) for an analysis of the differences in regional cloud feedback]. Both models show the fundamental role of the wind-driven latent heat flux changes in initiating the composite warm event. HadGEM1 simulates a strong positive cloud feedback that contributes to the growth of the event, while in CCCma T63 the cloud radiation anomaly is absent and the SST tendency is dominated by the latent heat flux anomaly throughout the event. Note as well that the magnitude of the warming is larger in the HadGEM1.

In addition, Clement et al. (2011) showed that the variance of the thermally coupled Walker mode is model dependent (see Table 1). Here we test whether differences in the simulation of the cloud feedback can explain the intermodel difference of the TCW magnitude. We estimate the strength of the cloud feedback in the EESSP (20°S ~ 10°N, 120° ~ 80°W) by regressing the cloud radiation anomaly onto the SST anomaly for each model and plot the regression coefficients against the standard deviations of the TCW (see the Table 1 caption for the definition). The results in Fig. 5 show a positive correlation across models between the cloud feedback and the TCW variance: the stronger the positive cloud feedback is, the larger the TCW variability will likely be.

The domain-averaged composite heat budget analysis was also carried out in the western-central Pacific (WCP) around the date line (10°S ~ 0°, 160°E ~ 160°W) (Fig. 4d), and shows a different role for clouds in that region. The variability in the west Pacific is much weaker than that in the EESSP (cf. Fig. 4a). The growth of the surface warming is initially dominated by the positive cloud radiation anomaly (blue curve) and then by the positive latent heat flux anomaly (green curve), which is driven by reduced winds (gray curve). The cloud radiation anomaly becomes negative as the SST anomaly increases owing to the increase in cloud fraction, and this balances the latent heat flux warming. As a result of this negative cloud feedback (which all models simulate), the SST anomaly is smaller in the western Pacific than the east. This contrast contributes to the SST gradient, which weakens the winds, maintaining the event. The maximum surface warming in the WCP lags behind the SE Pacific, consistent with the northwestward propagation of the surface warming originating in the SE Pacific via the WES feedback illustrated in Fig. 2.

Although the mechanisms illustrated above are derived directly from the composite warm events, they operate in cold events similarly, though in an opposite manner (not shown). It is noteworthy that a warm

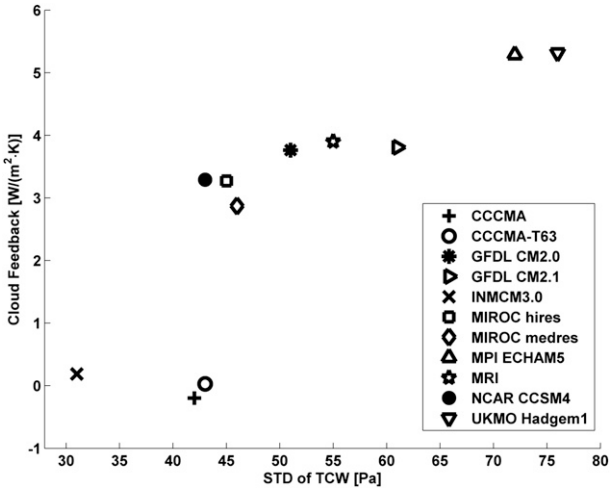

FIG. 5. Scatterplot of the cloud feedback estimated in the EESSP (10°N ~ 20°S, 120° ~ 80°W) vs the standard variation of the TCW (see Table 1 captions for the definition) for the 11 AGCM-slab models listed in Table 1. The cloud feedback in the EESSP is estimated by regressing the cloud radiation anomaly onto the SST anomaly in each model.

SPMM event does not necessarily lead to a cold event, and vice versa. This is unlike ENSO where El Niño tends to overshoot to La Niña because of interactive ocean dynamics (Jin 1997) that is absent in the AGCM-slab models.

The composite analysis demonstrates that the off-equatorial trade wind variability in the SE Pacific plays a fundamental role in the development of the SPMM. What triggers the southeast trade wind variability? In the low-pass filtered composite warm event, the southeast trade wind weakening is associated with an anomalous cyclone in the SE subtropical Pacific (Fig. 2a, $t = -12$). This anomalous cyclone seems to be related to a wave-train-like pattern extending southeastward from the western Pacific–Australia region, which suggests a possible remote forcing of the southeast trade wind variability from the tropics via Rossby wave dynamics (e.g., Lachlan-Cope et al. 2001; Lachlan-Cope and Connolley 2006; Ding et al. 2011; Jin and Kirtman 2009). However, in both the unfiltered and high-pass filtered composites (not shown), there is no large-scale wave train pattern prior to the southeast trade wind weakening. Rather the weaker trades on a shorter time scale are associated with a more regional-scale cyclonic anomaly, suggesting that local internal atmospheric dynamics may also contribute to the southeast trade wind variability, as suggested by Okumura (2013). This is more akin to the ideas on the origin of northern meridional modes, where it is argued that internal atmospheric variability (i.e., the North Pacific/Atlantic Oscillation) is the main driver of trade wind variability associated with the NPMM and the Atlantic meridional mode (Chiang and Vimont 2004; Nobre and Shukla 1996). A quantitative assessment of the relative importance of the remote tropical forcing versus the local internal atmospheric dynamics in triggering the SPMM events is not possible with the data used in this study but requires additional sensitivity experiments where these two forcings should be removed and evaluated separately. This will be investigated in another study.

Although sharing nearly identical physical mechanisms, the SPMM and the NPMM exhibit some noticeable differences. The most interesting, as mentioned earlier in this section, is their different impacts on the equatorial Pacific in terms of both magnitude and spatial structure. This difference in the AGCM-slab models is likely associated with the distribution of mean surface winds that determines the spatial extent to which the WES feedback can reach (Liu and Xie 1994). Background trade winds simulated in the AGCM-slab models (Fig. 6) converge in the eastern Pacific to the north of the equator at the intertropical convergence zone (ITCZ, around 8°N), which favors the northward extension of the SPMM into the deep tropics yet keeps the NPMM from developing onto the equator. This hypothesis has a theoretical support from an analytical study by Wang (2010b) and is further supported by the fact that the border between the SPMM and the NPMM in the AGCM-slab models (top row, Fig. 1) is nearly collocated with the ITCZ. In fact, it is the northward extension of the SPMM that leads to the ENSO-like variability in the absence of ocean–atmosphere dynamical coupling.

c. *SPMM in fully coupled climate models and observations*

In this section we examine whether the SPMM operates in fully coupled climate models and observations. As for the AGCM-slab models (Figs. 1a,b), we first calculate the regressions for the fully coupled climate models and observations. In the South Pacific, both regression patterns (Figs. 1d,f) exhibit the basic characteristics of the SPMM identified in the AGCM-slab models, which include the weakening southeast trade winds, the wedge-like SST warming below, as well as the zonal gradient in SLP resembling Southern Oscillation. These features remain robust (patterns are very similar to Fig. 1b, not shown) when we linearly remove ENSO impacts by subtracting the regression onto the cold tongue index as in Chiang and Vimont (2004). Then we perform the composite analysis in the fully coupled models and observations. As in the AGCM-slab models, the composites in the fully coupled models indicate

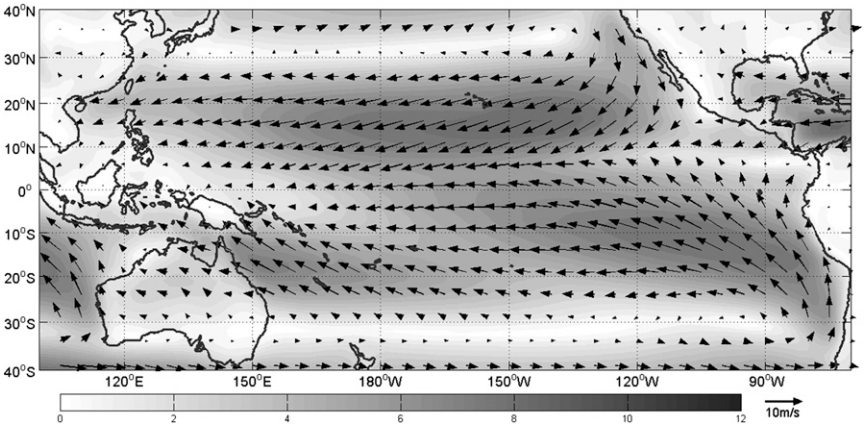

FIG. 6. Multimodel-mean surface winds in the AGCM-slab models: the grayscale indicates wind speed. Note the ITCZ is located around 8°N in the eastern Pacific.

similar northwestward development of the SE Pacific SST and SLP anomalies (Fig. 3b), which implies the wind–evaporation–SST feedback, as well as similar roles of the southeast trade winds and latent heat fluxes during the development (not shown). The observed composite Hovmöller diagrams (Figs. 3c,d), calculated from two different SST datasets [ERSST and Hadley Centre Sea Ice and Sea Surface Temperature dataset (HadISST)], also show similar northwestward propagation of the anomalous SST and SLP in the SE Pacific, as in the AGCM-slab models. All of these results suggest that the SPMM, although identified in the AGCM-slab models, should be active in the fully coupled models and observations as well.

There are, however, significant differences in the presence of interactive ocean dynamics. First of all, as shown by the regressions (Figs. 1d,f), the equatorial warming signal is significantly enhanced in both fully coupled models and observations. This enhanced equatorial signal also appears in the composites (Figs. 3b–d) but lags behind the SE Pacific surface warming peak by about 2 months in the fully coupled models, about 5–6 months in ERSST, and about 3–4 months in HadISST. This phase lag suggests that the South Pacific subtropical variability can propagate into the tropical Pacific via the SPMM and then be enhanced by ENSO dynamics. In other words, the SPMM can potentially serve as a trigger of ENSO events, as previous studies have suggested that the NPMM can trigger ENSO events (Chang et al. 2007). We note, however, that in the fully coupled models the composite equatorial warming starts around the same time as the SE Pacific surface warming (Fig. 3b), which is different from the AGCM-slab models where the equatorial warming lags the SE Pacific warming (Fig. 3a). This suggests that the equatorial warming in the AGCM-slab models originates primarily from the South Pacific extratropics; while in the fully coupled models the equatorial warming not only originates from the South Pacific, but also arises from other regions such as the local tropical Pacific. In both observational datasets, especially ERSST, this feature of the early onset of the equatorial warming is not as apparent as in the fully coupled models (Figs. 3c,d versus Fig. 3b), implying that those models may either underestimate the potential role of the SPMM in triggering ENSO events or overestimate other triggers of ENSO such as local atmospheric noise.

Another difference that appears in both fully coupled models and observations is the shorter persistence of the equatorial warming than in the AGCM-slab models. This is expected given the restoring influence of the interactive ocean dynamics, which overshoot to produce a La Niña one year later (Jin 1997).

In the previous section, we discussed the difference between the SPMM and the NPMM in the AGCM-slab models. Here we reexamine this issue in the fully coupled models and observations by calculating the regressions for the NPMM in the same manner as in Fig. 1a and comparing them to those associated with the SPMM. As expected, the main features of the NPMM are reproduced in both fully coupled models (Fig. 1c) and observations (Fig. 1e). Further, both equatorial warming signals in Figs. 1c,e are enhanced compared to the AGCM-slab models, consistent with the findings of Chang et al. (2007) that the NPMM can trigger ENSO events. However, for the same unit standard deviation of the SST indices in the North Pacific and South Pacific used in the regression, the equatorial warming signal associated with the NPMM is much weaker than that associated with the SPMM in both fully coupled models and observations (Figs. 1c,e versus Figs. 1d,f), suggesting

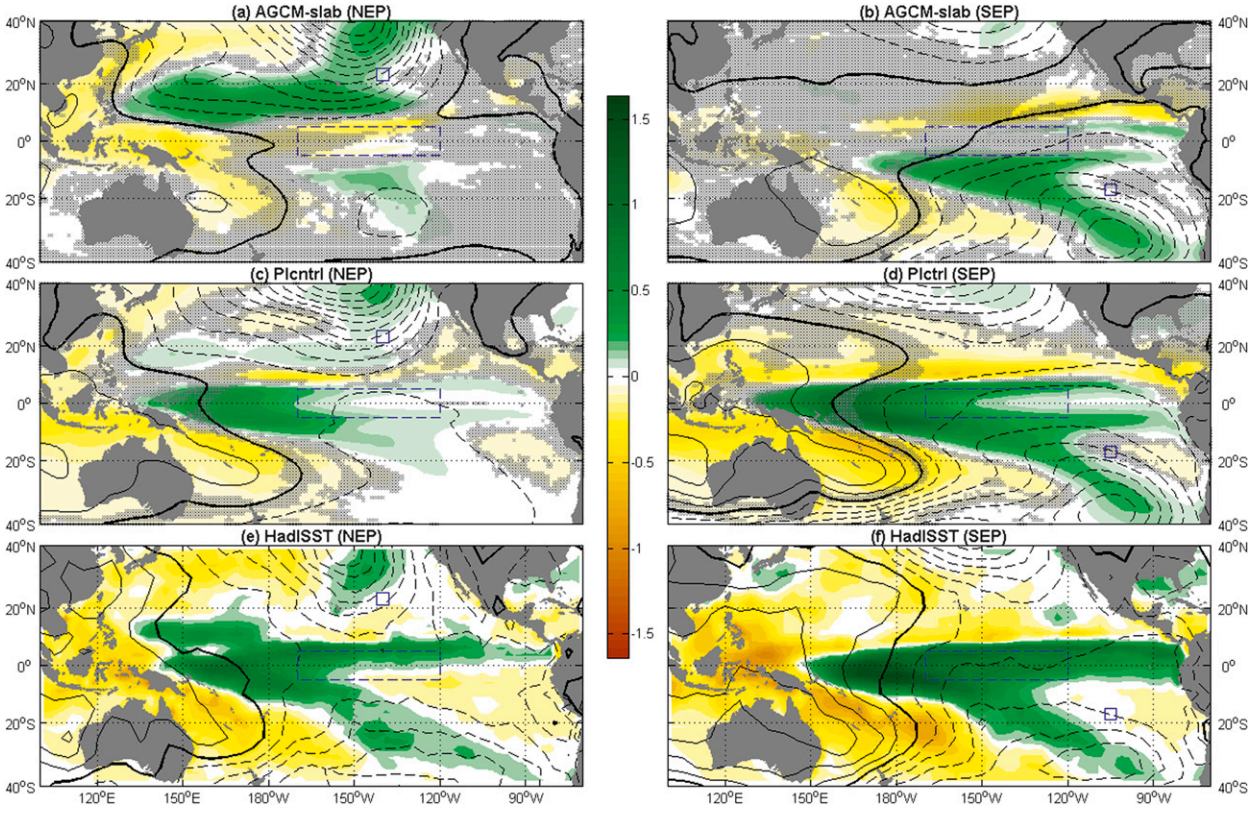

FIG. 7. As in Fig. 1, but for precipitation (shading) and SLP (contours). The SLP contours are the same as those in Fig. 1 and are repeated here for reference. The observed precipitation is from Global Precipitation Climatology Project, version 2.2, with a temporal coverage from 1979 to 2011. Results based on NOAA ERSST are similar.

a *stronger* coupling of the tropical Pacific to the South Pacific than to the North Pacific (Matei et al. 2008). In addition, in the fully coupled models, and particularly in the observations, the equatorial warming signal associated with the NPMM is more significant in the central to west Pacific, as in central Pacific El Niño events (Kao and Yu 2009), while for the SPMM it is larger in the central to east Pacific and similar to canonical El Niño events. This suggests that the NPMM and the SPMM may be related with different ENSO flavors. These differences in the fully coupled models and observations are consistent with the different equatorial impacts of the SPMM and the NPMM in the AGCM-slab models described before.

Another noticeable difference between the SPMM and the NPMM that appears in all AGCM-slab models, fully coupled models, and observations is that the SLP regressions in Fig. 1 are more hemispherically symmetric for the SPMM than for the NPMM. An anomalous North Pacific low pressure emerges with the SPMM even in the AGCM-slab models (second column, Fig. 1), while there is little corresponding signal in the South Pacific for the NPMM (first column, Fig. 1). Our interpretation is that the SLP signal appearing in the North Pacific is the atmospheric response to the tropical precipitation changes (as in Deser et al. 2004; Deser and Phillips 2006) that are triggered by the SPMM and amplified by the ocean–atmospheric dynamical coupling. Figure 7 shows the same regressions as in Fig. 1 but for precipitation and SLP. In the AGCM-slab models, the precipitation anomaly is quite weak on the equator, and there is a weak response in the North Pacific (Fig. 7b). With the ocean–atmosphere dynamical coupling, the equatorial precipitation signal is stronger, and the SLP pattern is more hemispherically symmetric in both fully coupled models and observations (Figs. 7d,f). The above explanation also applies to the SLP and precipitation regressions associated with the NPMM in Fig. 7, which, despite being weaker than those associated with the SPMM, indicates a larger precipitation signal on the equator and a more significant low pressure in the South Pacific with the presence of the dynamical coupling (Figs. 7c,e versus Fig. 7a).

d. Seasonality

In this section, we investigate the seasonality of the SPMM by examining the monthly variance of the SEP

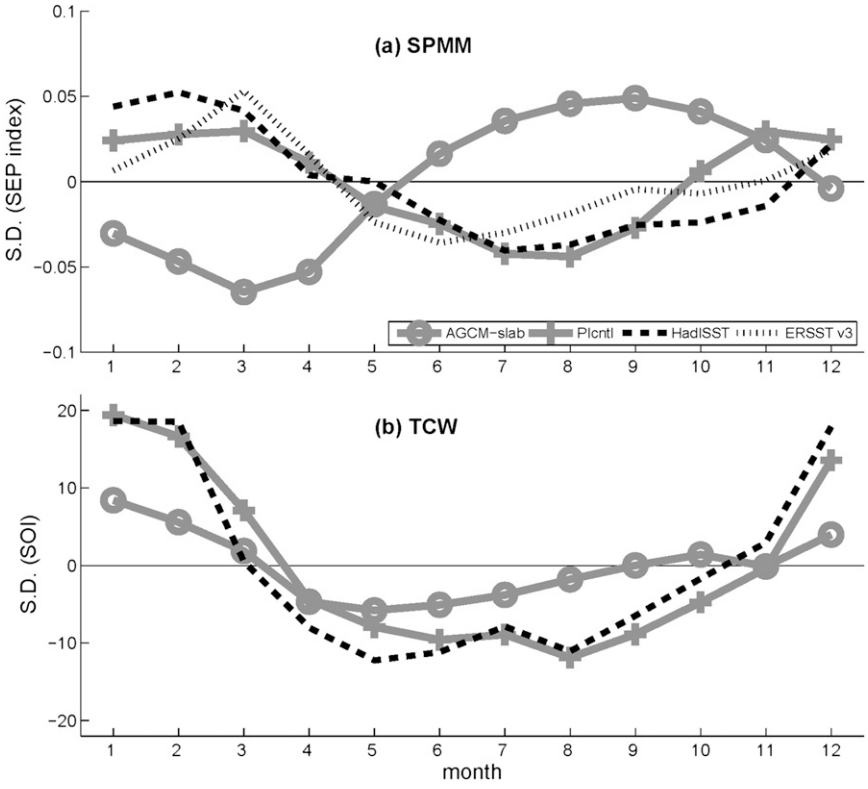

FIG. 8. Seasonality of the (a) SPMM and (b) TCW in the AGCM-slab models (gray lines with circles, multimodel mean), fully coupled models (gray lines with crosses, multimodel mean), and observations (HadISST in black dashed lines and ERSST v3 in black dotted line) expressed by the standard deviation of the SEP and Southern Oscillation indices as a function of calendar month. The mean standard deviation for all months is removed to emphasize the seasonality. The SO index is defined as the monthly sea level pressure difference between 5°S–5°N, 100°E–180° and 5°S–5°N, 90°–140°W. Observations are detrended. No low-pass filter is applied.

index used in the composite analysis. Before presenting the results, we note that the SEP index is a reasonable metric for the SPMM seasonality in the AGCM-slab models since ENSO is absent. In the fully coupled models and observations, however, the SEP index can only provide a qualitative description of the SPMM seasonality owing to the presence of ENSO and local ocean dynamics, which should also impact the SEP index variability.

Figure 8a shows the monthly standard deviation of the SEP index in three types of datasets. In the AGCM-slab models (gray circle curve, multimodel mean), the SEP index exhibits greatest variability during austral early spring (August to October). This is expected since the mixed layer depth is fixed in the AGCM-slab models and the SST variation is dominated by atmospheric activity, which is presumably stronger during cold seasons. In contrast, the seasonality of the SEP index peaks during austral summer (December to March) in the fully coupled models (gray cross curve, multimodel mean) and observations (HadISST in black dashed and ERSST v3 in black dotted curves). One explanation for this result, consistent with the observational study by Terray (2010, Fig. 2 therein), is the seasonal variation of the ocean mixed layer depth: a smaller thermal inertia of the summertime mixed layer associated with its shallower depth can lead to a larger SST change even given a relatively weaker summertime atmospheric forcing (Terray 2010). In addition, as mentioned above, ENSO, which is strongest in austral summer, may also contribute to the austral summer peak of the SEP index variability in the fully coupled models and observations.

Also shown in Fig. 8 is the seasonality of the Southern Oscillation index (SOI) (bottom panel). In the AGCM-slab models (gray circle curve), the SOI has a larger variability in austral summer (December to February), which lags behind that of the SEP index (Fig. 8a) by about a season. This supports our argument that the South Pacific meridional mode propagates into the deep tropics and leads to the ENSO-like variability in the AGCM-slab models (or TCW). In the presence of the

ocean–atmosphere dynamical coupling (gray cross curve and black dashed curve in Fig. 8b), the seasonality of the SOI is similar to, yet stronger than, the AGCM-slab models. As shown by Clement et al. (2011), the thermally coupled Walker mode has almost the same seasonality as the observed SO. This result provides a possible interpretation of the ENSO seasonality from the Southern Hemisphere and is consistent with the hypothesis by Liu and Xie (1994) that a substantial part of the equatorial seasonal variability may come from the extratropics on the basis of a simple coupled ocean–atmosphere boundary model.

4. Summary and discussion

The impact of mid-to-high latitude intrinsic variability on the tropical climate has been explored in previous studies but with a focus on the Northern Hemisphere. In this study, we investigate the role of South Pacific mid-to-high latitude variability in the tropical Pacific climate by performing the composite heat budget analysis in multiple AGCM-slab models where dynamical coupling between the atmosphere and ocean, responsible for ENSO, is excluded. A robust mode of variability thermodynamically connecting the South and tropical Pacific, defined as the South Pacific meridional mode, has been identified in the AGCM-slab models. The physical interpretation of the SPMM is nearly identical to the North Pacific meridional mode, and the underlying processes involve the Pacific southeast trade wind variability triggered by mid-to-high latitude atmospheric variability in the South Pacific and/or remote forcing in the tropics, its effects on SST by modulating latent heat fluxes, a positive cloud feedback contributing to the growth of the SPMM, and a wind–evaporation–SST feedback responsible for the northwestward extension of the SPMM onto the equator. Like the NPMM, the SPMM does not have an intrinsic time scale. The SPMM together with the well-established NPMM and North Atlantic meridional mode function as an effective conduit through which the mid-to-high latitude atmospheric variability impacts the equatorial climate.

The positive cloud feedback for the SPMM in the east equatorial–southern subtropical Pacific is not simulated by all AGCM-slab models and, thus, is not fundamental to the SPMM that emerges in all models. However, differences in the strength of the positive cloud feedback simulated by these AGCM-slab models to a large extent account for the intermodel difference of ENSO-like variability in magnitude as shown by Clement et al. (2011), implying its substantial role in the effectiveness of the SPMM in conveying the southern extratropical atmospheric variability into the equatorial Pacific. Types of clouds involved in the positive cloud feedback are model dependent owing to different cloud parameterizations in the CMIP3 models. Nonetheless, a new study by Bellomo et al. (2013) suggests that there is observational support for a positive feedback between SST and low-level clouds in the stratus regions including the northeast Pacific and northeast Atlantic Oceans, as well as the southeast Atlantic where there is sufficient data. They also show that the observed positive low-level cloud feedback in the eastern ocean basins is much stronger than that simulated by the CMIP5 (phase 5) models, suggesting that the amplitude of these modes of Pacific variability may be too weak in current climate models. In addition, this positive low-level cloud feedback in the SE Pacific has also been invoked to explain the observed annual march of the eastern Pacific cold tongue (Mitchell and Wallace 1992).

In the western Pacific, the SST anomaly is much weaker and lags behind that in the SE Pacific. This smaller magnitude is due to the role of cloud radiation and latent heat flux, which is different from that in the southeast and eastern equatorial Pacific. The surface variability in the western equatorial Pacific is initially driven by the cloud radiation anomaly and then mainly by the latent heat flux anomaly associated with the WES feedback. A negative cloud feedback in that region limits the surface warming and, hence, emphasizes the zonal asymmetry of the equatorial signature of the SPMM. The different roles of cloud radiation and latent heat flux in the surface variability in the east and west basins in large part account for the zonal asymmetry of the SPMM. This is consistent with previous studies by Kitoh et al. (1999) and Dommenget (2010).

Although sharing nearly the same physical mechanisms, the SPMM and NPMM also have some noticeable differences. The most significant is that the NPMM is more confined to the Northern Hemisphere with little influence on the western equatorial Pacific, while the SPMM extends more into the deep tropics, especially the central to east equatorial Pacific. This difference is apparent in the AGCM-slab models, fully coupled models, and observations and is likely related with the background field in the eastern Pacific. Southeast trade winds cross the equator in the eastern basin (Fig. 6), which favors the northward development of the SPMM even beyond the equator via the WES feedback in the AGCM-slab models. This hypothesis has theoretical support from an analytical study by Wang (2010b). In fully coupled models and observations, besides the WES feedback, the Pacific cold-tongue-related ocean dynamics (say, mean advection) may also contribute to the northward extension of the SPMM (Mitchell and Wallace 1992; Liu and Xie 1994). As a result, the SPMM

directly modulates the zonal gradients of SST and SLP on the equator and leads to the ENSO-like variability in the absence of ocean–atmosphere dynamical coupling. The NPMM also shows an effect on the equatorial Pacific climate, yet the effect is much smaller. Further, in fully coupled models and observations the SPMM and the NPMM seem to be related with different ENSO flavors: the equatorial signature of the SPMM is more reminiscent of the canonical El Niño while that associated with the NPMM is more like the central Pacific El Niño.

The origin of the ENSO-like variability in the absence of dynamical coupling suggested in this study is consistent with the hypothesis by van Loon and Shea (1985), who argued that the Southern Oscillation originates in the South Pacific. However, the proposed processes in these two studies are somewhat different. In their study, changes of the trough in the westerlies at the surface over the South Pacific lead to anomalous meridional winds and SST between 15° and 45°S west of 140°W, which enhances or reduces deep convection within the SPCZ. The anomalous convection is suggested to be responsible for the SLP anomalies associated with the SO over large parts of the tropical and subtropical South Pacific. Here we showed that the off-equatorial trade wind variability in the SE Pacific (about east of 140°W) initiates the SPMM that eventually develops into the ENSO-like variability. Because there is no preferred time scale of the SPMM, we interpret this trade wind variability as arising primarily from stochastic forcing from the midlatitudes (i.e., internally generated atmospheric variability). Our results do show an anomalous SPCZ associated with the SPMM in Fig. 7 (the second column), indicated by the eastward shift of the precipitation band in the South Pacific. This may contribute to the development of the anomalous SLP in the SE subtropical Pacific shown in the composite heat budget analysis (recall Fig. 2).

The SPMM presented in this study shares similar spatial patterns to the observed subtropical dipole mode (STDM) in the South Pacific (e.g., Wang 2010a) that exhibits a northeast–southwest-tilted SST dipole pattern (similar to Fig. 2a, $t = 0$). This resemblance seems to imply that these two modes may describe the same climate variability. However, there exist a couple of fundamental differences between the SPMM and the STDM. First of all, the STDM in the literature has a characteristic time scale of about a season, while the SPMM here operates on various time scales ranging from seasonal to interannual and longer time scales. Secondly, the SPMM is a propagating mode that transports the extratropical South Pacific variability into the tropics (which is the reason why we define it as a meridional mode). In contrast, the STDM has been described as a standing mode in the subtropical South Pacific. While it is possible that the STDM is a snapshot of the propagating SPMM on the seasonal time scale, a comprehensive comparison of these two modes is needed and is beyond the scope of this work.

Results from fully coupled models and observations indicate that a similar WES feedback operates and propagates signals from the SE Pacific into the equatorial region as in the AGCM-slab models, which demonstrate an active role for the SPMM in the fully coupled climate models and the real world. Further, the enhanced equatorial ENSO-like signal peaks behind the SE Pacific variability, suggesting that the South Pacific extratropical variability could trigger ENSO events via the SPMM. It is noteworthy that Jin and Kirtman (2009), based on evidence from both observations and models, argued that, although the observed atmospheric variability in the South Pacific (i.e., the Pacific–South America pattern) peaks one season before the ENSO peak, it is actually a response to the developing ENSO forcing. This notion seems to contradict our argument that the South Pacific extratropical variability can trigger ENSO events. However, these two arguments can be reconciled in that the forcing of the South Pacific atmospheric variability, in the fully coupled models and observations, could include both local internal dynamics and remote tropical forcing. The local part of the South Pacific extratropical atmospheric variability can trigger ENSO events via the SPMM, while the remotely forced part from ENSO may still propagate onto the equator via the SPMM and interact with ENSO (Toniazzo 2009). Whether the SPMM originates solely from the South Pacific extratropics or partly from the remote tropical forcing, especially in the fully coupled models and observations, needs further study.

This study highlights the important role of the Southern Hemisphere atmospheric variability in the tropical Pacific climate and suggests that including observations from the data-poor South Pacific could potentially improve the ENSO predictability.

Acknowledgments. We acknowledge Clara Deser, Chunzai Wang, Lixin Wu, Qinyu Liu, Michelle L'Heureux, and Ben Kirtman for their insightful suggestions and Bob Tomas for his help in providing NCAR CCSM4 simulations. Comments from anonymous reviewers are helpful to improve the original manuscript. We would also like to thank the various international modeling groups participating in CMIP3. NCEP Reanalysis and GPCP data is provided by the NOAA/OAR/ESRL PSD, Boulder, Colorado (from their website at http://www.esrl.noaa.gov/psd/). This work was funded by NOAA, U.S. DOE, and by NSF Climate and Large-Scale Dynamics Program.

REFERENCES

Adler, R. F., and Coauthors, 2003: The version 2 Global Precipitation Climatology Project (GPCP) monthly precipitation analysis (1979–present). *J. Hydrometeor.,* **4,** 1147–1167.

Barnett, T. P., D. W. Pierce, M. Latif, D. Dommenget, and R. Saravanan, 1999: Interdecadal interactions between the tropics and midlatitudes in the Pacific basin. *Geophys. Res. Lett.,* **26,** 615–618.

Bellomo, K., A. C. Clement, J. R. Norris, and B. J. Soden, 2013: Observational and model estimates of cloud amount feedback over the Indian and Pacific Oceans. *J. Climate,* in press.

Chang, P., L. Ji, and H. Li, 1997: A decadal climate variation in the tropical Atlantic Ocean from thermodynamic air–sea interactions. *Nature,* **385,** 516–518.

——, L. Zhang, R. Saravanan, D. J. Vimont, J. C. H. Chiang, L. Ji, H. Seidel, and M. K. Tippett, 2007: Pacific meridional mode and El Niño–Southern Oscillation. *Geophys. Res. Lett.,* **34,** L16608, doi:10.1029/2007GL030302.

Chiang, J. C. H., and D. J. Vimont, 2004: Analogous Pacific and Atlantic meridional modes of tropical atmosphere–ocean variability. *J. Climate,* **17,** 4143–4158.

Clement, A. C., R. Burgman, and J. Norris, 2009: Observational and model evidence for positive low-level cloud feedback. *Science,* **325,** 460–464, doi:10.1126/science.1171255.

——, ——, and ——, 2010: Response to comment on ''Observational and model evidence for positive low-level cloud feedback.'' *Science,* **329,** 277.

——, P. DiNezio, and C. Deser, 2011: Rethinking the ocean's role in the Southern Oscillation. *J. Climate,* **24,** 4056–4072.

Compo, G. P., and P. D. Sardeshmukh, 2010: Removing ENSO-related variations from the climate record. *J. Climate,* **23,** 1957–1978.

Deser, C., and A. S. Phillips, 2006: Simulation of the 1976/77 climate transition over the North Pacific: Sensitivity to tropical forcing. *J. Climate,* **19,** 6170–6180.

——, ——, and J. W. Hurrell, 2004: Pacific interdecadal climate variability: Linkages between the tropics and the North Pacific during boreal winter since 1900. *J. Climate,* **17,** 3109–3124.

Ding, Q., E. J. Steig, D. Battisti, and M. Kuttel, 2011: Winter warming in west Antarctic caused by central tropical Pacific warming. *Nat. Geosci.,* **4,** 398–403.

Dommenget, D., 2010: A slab ocean El Niño. *Geophys. Res. Lett.,* **37,** L20701, doi:10.1029/2010GL044888.

Jin, D., and B. P. Kirtman, 2009: Why the Southern Hemisphere ENSO responses lead ENSO. *J. Geophys. Res.,* **114,** D23101, doi:10.1029/2009JD012657.

Jin, F.-F., 1997: An equatorial ocean recharge paradigm for ENSO. Part I: Conceptual model. *J. Atmos. Sci.,* **54,** 811–829.

Kalnay, and Coauthors, 1996: The NCEP/NCAR 40-Year Reanalysis Project. *Bull. Amer. Meteor. Soc.,* **77,** 437–470.

Kao, H.-Y., and J.-Y. Yu, 2009: Contrasting eastern-Pacific and central-Pacific types of ENSO. *J. Climate,* **22,** 615–632.

Kitoh, A., T. Motoi, and H. Koide, 1999: SST variability and its mechanism in a coupled atmosphere–mixed layer ocean model. *J. Climate,* **12,** 1221–1239.

Lachlan-Cope, T. A., and W. M. Connolley, 2006: Teleconnections between the tropical Pacific and the Amundsen-Bellinghausens Sea: Role of the El Niño/Southern Oscillation. *J. Geophys. Res.,* **111,** D23101, doi:10.1029/2005JD006386.

——, ——, and J. Turner, 2001: The role of the nonaxisymmetric Antarctic orography in forcing the observed pattern of variability of the Antarctic climate. *Geophys. Res. Lett.,* **28,** 4111–4114.

Liu, Z., and S.-P. Xie, 1994: Equatorward propagation of coupled air–sea disturbances with application to the annual cycle of the eastern tropical Pacific. *J. Atmos. Sci.,* **51,** 3807–3822.

Matei, D., N. Keenlyside, M. Latif, and J. Jungclaus, 2008: Subtropical forcing of tropical Pacific climate and decadal ENSO modulation. *J. Climate,* **21,** 4691–4709.

Mitchell, T. P., and J. M. Wallace, 1992: On the annual cycle in equatorial convection and sea surface temperature. *J. Climate,* **5,** 1140–1156.

Nobre, P., and J. Shukla, 1996: Variations of sea surface temperature, wind stress, and rainfall over the tropical Atlantic and South America. *J. Climate,* **9,** 2464–2479.

Okumura, Y., 2013: Origins of tropical Pacific decadal variability: Role of stochastic atmospheric forcing from the South Pacific. *J. Climate,* in press.

Pierce, D. W., T. P. Barnett, and M. Latif, 2000: Connections between the Pacific Ocean tropics and midlatitudes on decadal timescales. *J. Climate,* **13,** 1173–1194.

Rayner, N. A., D. E. Parker, E. B. Horton, C. K. Folland, L. V. Alexander, and D. P. Rowell, 2003: Global analyses of SST, sea ice, and night marine air temperature since the late nineteenth century. *J. Geophys. Res.,* **108,** 4407, doi:10.1029/2002JD002670.

Rogers, J. C., 1981: The North Pacific Oscillation. *J. Climatol.,* **1,** 39–57.

Smith, T. M., R. W. Reynolds, T. C. Peterson, and J. Lawrimore, 2008: Improvements to NOAA's historical merged land–ocean surface temperature analysis (1880–2006). *J. Climate,* **21,** 2283–2296.

Terray, P., 2010: Southern Hemisphere extratropical forcing: A new paradigm for El Niño–Southern Oscillation. *Climate Dyn.,* **36,** 2171–2199, doi:10.1007/s00382-010-0825-z.

——, and S. Dominiak, 2005: Indian Ocean sea surface temperature and El Niño–Southern Oscillation: A new perspective. *J. Climate,* **18,** 1351–1368.

Toniazzo, T., 2009: Climate variability in the south-eastern tropical Pacific and its relation with ENSO: A GCM study. *Climate Dyn.,* **34,** 1093–1114, doi:10.1007/s00382-009-0602-z.

van Loon, H., and D. J. Shea, 1985: The Southern Oscillation. Part IV: The precursors south of 15°S to the extremes of the oscillation. *Mon. Wea. Rev.,* **113,** 2063–2074.

——, G. A. Meehl, and R. F. Millif, 2003: The Southern Oscillation in the early 1990s. *Geophys. Res. Lett.,* **30,** 1478, doi:10.1029/2002GL016307.

Vimont, D. J., D. S. Battisti, and A. C. Hirst, 2001: Footprinting: A seasonal connection between the tropics and mid-latitudes. *Geophys. Res. Lett.,* **28,** 3923–3926.

——, ——, and ——, 2003a: The seasonal footprinting mechanism in the CSIRO general circulation models. *J. Climate,* **16,** 2653–2667.

——, J. M. Wallace, and D. S. Battisti, 2003b: The seasonal footprinting mechanism in the Pacific: Implications for ENSO. *J. Climate,* **16,** 2668–2675.

——, M. Alexander, and A. Fontaine, 2009: Midlatitude excitation of tropical variability in the Pacific: The role of thermodynamic coupling and seasonality. *J. Climate,* **22,** 518–534.

Wang, F., 2010a: Subtropical dipole mode in the Southern Hemisphere: A global view. *Geophys. Res. Lett.,* **37,** L10702, doi:10.1029/2010GL042750.

——, 2010b: Thermodynamical coupled modes in the tropical atmosphere–ocean: An analytical solution. *J. Atmos. Sci.,* **67,** 1667–1677.

Xie, S. P., and S. G. H. Philander, 1994: A coupled ocean-atmosphere model of relevance to the ITCZ in the eastern Pacific. *Tellus,* **46A,** 340–350.

Zhang, Y., J. M. Wallace, and D. S. Battisti, 1997: ENSO-like interdecadal variability: 1900–93. *J. Climate,* **10,** 1004–1020.